Appl. Phys. A 91, 87–95 (2008)
DOI: 10.1007/s00339-007-4363-4

Applied Physics A
Materials Science & Processing

C. MASINGBOON[1]
S. MAENSIRI[1,✉]
T. YAMWONG[2]
P.L. ANDERSON[3]
S. SERAPHIN[3]

Nanocrystalline $CaCu_3Ti_4O_{12}$ powders prepared by egg white solution route: synthesis, characterization and its giant dielectric properties

[1] Small & Strong Materials Group (SSMG), Department of Physics, and Integrated Nanotechnology Research Center (INRC), Faculty of Science, Khon Kaen University, Khon Kaen 40002, Thailand
[2] National Metals and Materials Technology Center (MTEC), Thailand Science Park, Pathumthani 12120, Thailand
[3] Department of Materials Science and Engineering, The University of Arizona, Tucson, AZ 85721, USA

Received: 20 June 2007/Accepted: 19 November 2007
Published online: 19 December 2007 •

ABSTRACT Nanocrystalline $CaCu_3Ti_4O_{12}$ powders with particle sizes of 50–90 nm were synthesized by a simple method using $Ca(NO_3)_2 \cdot 4H_2O$, $Cu(NO_3)_2 \cdot 4H_2O$, titanium(diisoproproxide) bis(2,4-pentanedionate) and freshly extracted egg white (ovalbumin) in aqueous medium. The synthesized precursor was characterized by TG-DTA to determine the thermal decomposition and crystallization temperature which was found to be at above 400 °C. The precursor was calcined at 700 and 800 °C in air for 8 h to obtain nanocrystalline powders of $CaCu_3Ti_4O_{12}$. The calcined $CaCu_3Ti_4O_{12}$ powders were characterized by XRD, FTIR, SEM and TEM. Sintering of the powders was conducted in air at 1100 °C for 16 h. The XRD results indicated that all sintered samples have a typical perovskite $CaCu_3Ti_4O_{12}$ structure and a small amount of CuO, although the sintered sample of the 700 °C calcined powders contained some amount of $CaTiO_3$. SEM micrographs showed the average grain sizes of 12.0 ± 7.8 and 15.5 ± 8.9 μm for the sintered $CaCu_3Ti_4O_{12}$ ceramics prepared using the $CaCu_3Ti_4O_{12}$ powders calcined at 700 and 800 °C, respectively. The sintered samples exhibit a giant dielectric constant, ε' of ~ 1.5–5×10^4. The dielectric behavior of both samples exhibits Debye-like relaxation, and can be explained based on a Maxwell–Wagner model.

PACS 77.22.Gm; 81.05.Je; 81.07.Wx; 81.20.Ev

1 Introduction

Materials with high dielectric constant, good thermal stability and Ba/Pb-free are widely used in technological applications such as capacitors and memory devices. Recently, there has been a great interest in synthesis and characterization of a perovskite-type compound, $CaCu_3Ti_4O_{12}$, (abbreviated as CCTO) [1–15]. This non-ferroelectric material exhibits giant dielectric constant of $\varepsilon' \sim 10^4$ (for polycrystalline ceramics) [1, 2] and $\varepsilon' \sim 10^5$ (for single crystals) [3] in the kilohertz region over the temperature range from −173 to 327 °C. This material does not undergo any structural change over the same temperature range [1, 2] although its dielectric constant abruptly decreases to less than 100 below −173 °C and shows a Debye-like relaxation [13]. The characteristic relaxation frequency follows approximately the Arrhenius law. In addition to its interesting dielectric property, CCTO has remarkably strong linear current–voltage characteristics without the addition of dopants [16]. These excellent properties render this material particularly attractive for a wide range of applications.

So far, several models of the dielectric behavior of CCTO material have been proposed to be due to either intrinsic or extrinsic effect. Since the giant dielectric response of this material was found to be very sensitive to the microstructure (such as grain size) and processing conditions (such as sintering temperature and time, cooling rate, and partial pressure) [11–14, 17, 18], more investigations tend to believe that the high dielectric constant originates from the extrinsic effect, such as internal barrier layer capacitor (IBLC) [11, 17], contact-electrode effect [19, 20], and special inhomogenity of local dielectric response [21]. Although still unclear, the IBLC explanation of extrinsic mechanism is widely accepted [22–27].

CCTO powder was generally prepared by a standard solid-state reaction method [1–3]. This method requires tedious work and a high temperature in the powder preparation process. Moreover, it suffers from the disadvantages of inhomogeneity. In contrast, synthesis from a solution affords the reaction with a homogeneous mixing of the metal ions at the atomic scale, shorter reaction time, and at lower temperature in the powder preparation process [28].

However, it has been only a few reports on the solution methods to synthesize CCTO powders [8, 10, 13]. Therefore, alternative simple solution routes by utilization of cheap, nontoxic and environmentally benign precursors for preparation of CCTO powders are still a challenge. Egg white proteins are well known for their gelling, foaming and emulsifying characteristics, in addition to their high nutrition quality [29–31]. Due to its solubility in water and its ability to associate with metal ions in solution, egg white has been used as a binder cum gel forming material in shape form-

✉ Fax: +66-43-202374, E-mail: sanmae@kku.ac.th

ing of bulk and porous ceramics [32–34]. Egg white has been used as a matrix for entrapment of aluminum ions generating gel precursor which resulted in α-alumina particles with crystalline sizes of 15–80 nm after heat treatment as low as 330 °C [35]. Most recently, our group has reported the use of egg white solution for the preparations of plate-like clusters of CeO_2 nanocrystalline particles 6–30 nm in diameter [36] and nanoparticles of $NiFe_2O_4$ with particle sizes of 60–600 nm [37]. This method is simple, cost effective and environmental friendly, which is a promising synthesis route for preparation of fine ceramic particles.

In this study, we report the synthesis and giant dielectric properties of CCTO prepared by the simple egg white solution route using $Ca(NO_3)_2 \cdot 4H_2O$, $Cu(NO_3)_2 \cdot 4H_2O$, titanium(diisoproproxide) bis(2,4-pentanedionate) and freshly extracted egg white (ovalbumin) in aqueous medium. The synthesized fine CCTO powders were characterized by thermogravimetric and differential thermal analysis (TG-DTA), X-ray diffraction (XRD), Fourier-transform infared (FT-IR) spectroscopy, scanning electron microscopy (SEM) and transmission electron microscopy (TEM). The effects of particle size of the synthesized powders on microstructure and giant dielectric behavior of the sintered CCTO were also investigated.

2 Experimental procedure

The nanocrystalline CCTO powders were prepared by a simple egg white solution route. The procedures used to synthesize the CCTO powders were similar to those for the $NiFe_2O_4$ nanoparticles reported previously [37]. In a typical procedure, 60 ml of egg white was first mixed with 40 ml de-ionized water (3 : 2 ratio) under vigorous stir at room temperature (27 °C) until homogeneous solution was obtained. Subsequently, $Ca(NO_3)_2 \cdot 4H_2O$ (99.9% purity, Kento, Japan), $Cu(NO_3)_2 \cdot 4H_2O$ (99.5% purity, Carlo Erba Reacgenti, Italy), and 75 wt. % titanium(diisopropoxide) bis(2,4-pentanedionate) in 2-propanol (99%, Acros organics, USA) in a mole ratio corresponding to the nominal composition of $CaCu_3Ti_4O_{12}$. These chemicals were added to the egg white solution under vigorous stir at room temperature for 2 h to obtain a well-dissolved solution. At this step, the extracted egg white was acted as a matrix for entrapment of Ca, Cu, and Ti ions generating gel precursor [35–37]. Throughout the whole process described above, no pH adjustment was made. Then, the mixed solution was evaporated by heating on a hot plate at 100 °C under vigorous stir for several hours until dried precursor was obtained. The dried precursor was crushed into powder using mortar and pestle.

In order to determine the temperature of possible decomposition and crystallization of the nanoparticles, the dried precursor was subjected to thermogravimetric-differential thermal analysis (TG-DTA) (Pyris Diamond TG-DTA, Perkin–Elmer Instrument, USA). The crystallization seemed to occur at temperature above 400 °C (Fig. 1). The dried precursor then was calcined in box-furnace at 700 and 800 °C for 8 h in air. The calcined powder precursors were reground and passed through 106 μm sieve (Test sieve, Endecotts Limited, England) to break up large agglomerates.

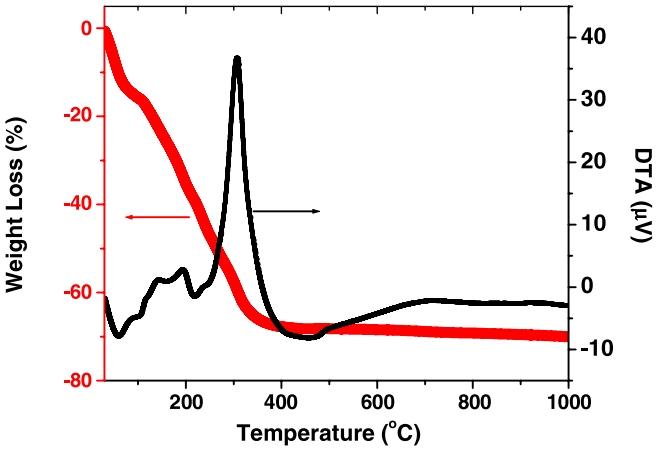

FIGURE 1 The TG/DTA curves of the thermal decomposition of $CaCu_3Ti_4O_{12}$ precursor at a heating rate of 15 °C/min in static air

The prepared CCTO powers were characterized by X-ray diffraction (PW3040 Philips X-ray diffractometer with Cu K_α radiation ($\lambda = 0.15406$ nm), The Netherlands), Fourier transform infrared spectrometer (Spectrum One FT-IR Spectrometer, Perkin–Elmer Instruments, USA), scanning electron microscopy (LEO SEM VP1450, UK) and transmission electron microscopy (TEM, Hitachi H8100 200 kV).

The prepared powders were pressed uniaxially in a 16 mm die with an applied pressure of 100 MPa. The compacts were pressureless-sintered at 1100 °C for 16 h in air in a box furnace with heating and cooling rates of 5 °C/min. The sintered disc samples of $\sim$ 14 mm in diameter with a thickness of $\sim$ 2 mm were obtained. The average grain size of each sintered CCTO ceramic was measured using a standard line intercept technique from SEM micrographs of sintered CCTO surfaces and counting at least 200 intercepts for each micrograph. Throughout this article, we assigned symbols of CCTO_EW700 and CCTO_EW800 for the sintered CCTO samples fabricated using the CCTO powders calcined at 700 and 800 °C, respectively.

The capacitance, C, and loss tangent, $\tan\delta$, were carried out as a function of frequency (100 Hz–10 MHz) and temperature (−50 to +190 °C), using a Hewlett Packard 4194A Impedance Gain Phase Analyzer at an oscillation voltage of 1 V. Each measured temperature was kept constant with an accuracy of ±1 °C. Silver paint was coated on both surface of the samples and dried over night. The complex permittivity, ε^*, was calculated as follows:

$$\varepsilon^* = \varepsilon' - i\varepsilon'' , \tag{1}$$

where

$$\varepsilon' = \frac{Cd}{\varepsilon_0 A} , \tag{2}$$

$$\varepsilon'' = \varepsilon' \tan\delta , \tag{3}$$

where ε_0 is the permittivity in free space, A is the sample area and d is the sample thickness. The values of ac conductivity, σ_{ac}, were derived from [38]:

$$\sigma_{ac} = \omega\varepsilon_0\varepsilon'' . \tag{4}$$

3 Results and discussion

The simultaneous TG-DTA curves of the gel precursor in flowing air are shown in Fig. 1. The TG curve in Fig. 1 shows a minor weight loss step between ~ 30 °C and 300 °C. A slight weight loss was observed between 300 and 400 °C, and almost no weight loss was observed at above 500 °C. The first weight loss (30–300 °C) is related to the losses of moisture, trapped solvent (water and carbon dioxide), alkoxide, and nitrates. A slightly weight loss was observed between 300 and 400 °C, relating to the losses of organic species associated in the precursor (the remaining organic mass in ovalbumin), or the residual carbon. Almost no weight loss could be observed at above 400 °C, suggesting the formation of crystalline CCTO as a decomposed product. This is confirmed by the XRD results as shown in Fig. 2. On the DTA curve (Fig. 1) three endothermic peaks were observed at ~ 57, 103, and 219 °C, respectively. The one exothermic was observed at 304 °C. The three endothermic peak confirms the combustion of water, whereas the one exothermic peak confirms that the thermal events was associated with the burnout of organic species involved in the precursor powders of the residual carbon or due to direct crystallization of CCTO from the amorphous component. No further weight loss and no thermal effect were observed above 400 °C, indicating that no decomposition occurs above this temperature. Note that this precursor was calcined in air at 700 and 800 °C for 8 h.

Figure 2 shows XRD patterns of (a) dried precursor and CCTO powders after calcination in air at (b) 700 °C and (c) 800 °C for 8 h. The main peaks of all calcined CCTO powders are comparable to those of the standard powder XRD pattern of CCTO in the JCPDS card No. 75-2188. In addition, the following phases of $CaTiO_3$ (JCPDS card No. 82-0228), CuO (JCPDS card No. 80-0076) and Anateses-TiO_2 (JCPDS card No. 78-2486) are also observed. It is suggested by Guilleemet-Fritsch et al. [39] that the pure CCTO phase is obtained only when the ratio of calcium, copper and titanium are close to the stoichiometric ones. The $CaTiO_3$ phase appears if an excess of titanium is present, and at the same time when the copper content slightly decreases. It is also suggested that the excess of titanium leads to the precipitation of $CaTiO_3$, even if there is no excess of calcium [39]. Since both calcium and titanium form a second phase, copper is then in excess, with respect with the stoichiometry of CCTO. Hence, the precipitation of the copper oxide (CuO) is observed, beside the CCTO and $CaTiO_3$ phase. From the line broadening of the main peaks, the crystallite size (D) was estimated using the Scherrer formula [40]:

$$D = K\lambda/(\beta\cos\theta)\,, \tag{5}$$

where λ is the wavelength of the X-ray radiation, K is a constant taken as 0.89, θ is the diffraction angle. β is the full width at haft maximum (FWHM) and is given by $\beta = (\beta_o^2 - \beta_i^2)^{1/2}$, where β_o and β_i are the widths from the observed X-ray peak and the width due to instrumental effects, respectively. The particle sizes are found to be 66.7 ± 27.5 and 86.2 ± 35.2 nm for the powders calcined at 700 and 800 °C, respectively. The values of lattice parameter a calculated from the XRD spectra were obtained to be 7.374 ± 0.002 and 7.390 ± 0.0005 Å for the CCTO powders calcined at 700 and 800 °C, respectively. The particle sizes and lattice parameters are also summarized in Table 1.

Figure 3 shows FT-IR spectra of the dried precursor and CCTO powders after calcination in air at 700 °C and 800 °C for 8 h. The calcined CCTO powders show the main

Material	Particle size from XRD (nm)	Particle size from TEM (nm)	Lattice parameter a (Å)
ASTM (75-2188)	–	–	7.391 ± 0.001
700 °C powders	66.7 ± 27.5	56.7 ± 7.9	7.374 ± 0.002
800 °C powders	86.2 ± 35.2	84.9 ± 15.3	7.390 ± 0.0005

TABLE 1 Summary of particle size analysis obtained from XRD and TEM; and lattice parameter (from XRD) of CCTO powders compared to the ASTM value

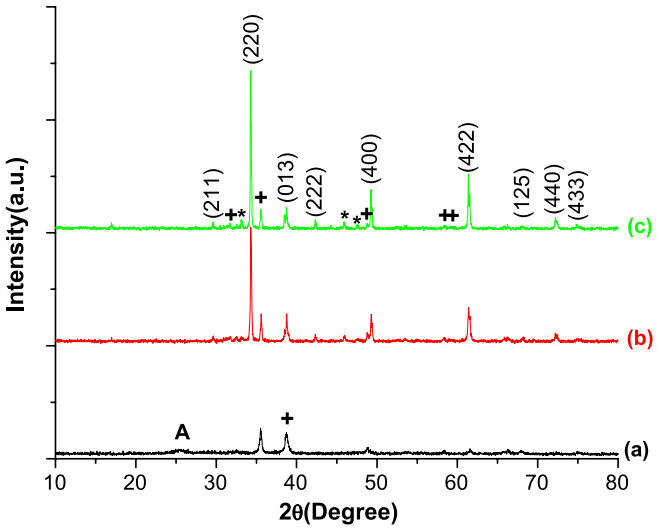

FIGURE 2 XRD patterns of (**a**) dried precursor and $CaCu_3Ti_4O_{12}$ nanopowders calcined in air for 8 h at (**b**) 700 °C, and (**c**) 800 °C. (* – $CaTiO_3$, + – CuO, A – Anatase-TiO_2)

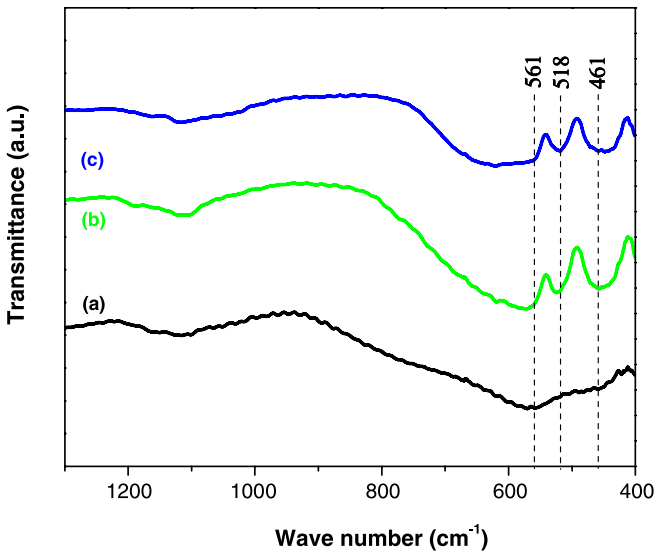

FIGURE 3 FT-IR patterns of (**a**) dried precursor and $CaCu_3Ti_4O_{12}$ nanopowders calcined in air for 8 h at (**b**) 700 °C, and (**c**) 800 °C

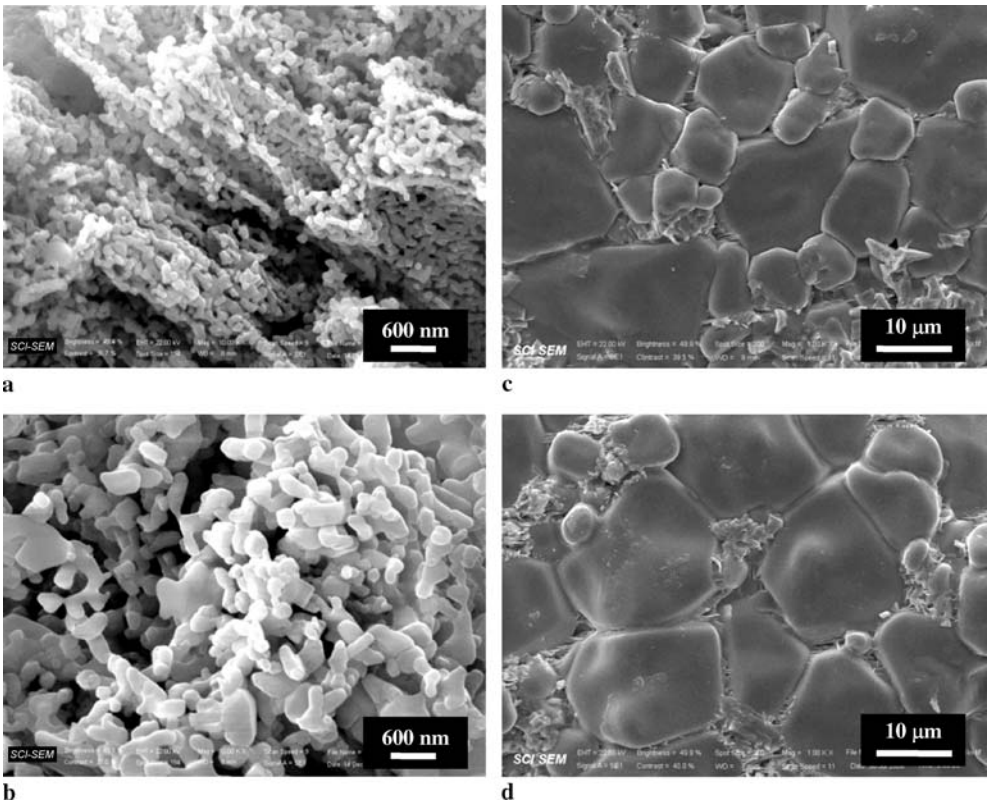

FIGURE 4 SEM micrographs of the CCTO powders and sintered CCTO materials. (**a**,**b**) are the powders calcined for 8 h in air at 700 °C and 800 °C, respectively. (**c**, **d**) are the microstructure of the sintering CCTO_EW700, and CCTO_EW800, respectively

absorption bands at 561, 516, and 437 cm^{-1}. These bands are assigned to the absorption regions for Ti ion, which are associated to ν_{Ti-O} of 653–550 cm^{-1} and (Ti−O−Ti of 495–436 cm^{-1}) [4, 41].

Morphology of the calcined CCTO powders and microstructure of the sintered CCTO ceramic samples revealed by SEM are shown in Fig. 4. Figure 4a and b show CCTO particles with sizes of about 60 nm, and 100 nm for the 700 °C and 800 °C calcined samples, respectively. These values were larger than those obtained from X-ray line broadening calculation. Some agglomerates were observed in all of the calcined powders. The particle size of the powder increased with increasing calcination temperature. After sintering at 1100 °C for 16 h, the bulk CCTO ceramics with different microstructure were obtained. The CCTO_EW700 (Fig. 4c) and CCTO_EW800 (Fig. 4d) showed mean grain sizes of 12.0 ± 7.8 μm and 15.5 ± 8.9 μm, respectively.

Figure 5 shows TEM images and the corresponding selected area electron diffraction (SAED) patterns of the calcined CCTO powders. It is clearly seen from the TEM bright-field images that both powder samples consist of nanocrystalline CCTO particles, whose size increases with increasing calcination temperature. The 700 °C calcined sample contains nanoparticles of 56.7 ± 7.9 nm in size whereas the 800 °C calcined sample contains nanoparticles of 84.9 ± 15.3 nm. The observed particle sizes are in good agreement with results determined from X-ray line broadening (see summary in Table 1). Electron diffraction of particles with higher calcination temperature contains more intense spots as shown in the 800 °C calcined powders, indicating the larger particle size of highly crystalline compared to the 700 °C calcined samples. The interplanar spacings (d_{hkl}) measured from the selected-area electron diffraction patterns are in good agreement with the values obtained from the standard data JCPDS: 75-2188 (for CCTO) and 89-0056 (for $CaTiO_3$) as summarized in Table 2.

Figure 6 shows XRD patterns of the CCTO ceramics sintered in air at 1100 °C for 16 h, confirming a main phase of CCTO and a small amount of CuO in both the CCTO_EW700 and CCTO_EW800 although a small amount of $CaTiO_3$ was present in the CCTO_EW700 sample. The presence of additional $CaTiO_3$ in the sintered CCTO_EW700 is possibly due to the presence of excess titanium on the powders, calcined at 700 °C. Guilleemet-Fritsch et al. [39] suggested that the titanium content mostly controls the phase composition (single or second phase material) of the CCTO materials. Therefore, we think that the excess of titanium leads to the precipitation of $CaTiO_3$ in our CCTO_EW700 sample. In the case of CCTO_EW800, however, the $CaTiO_3$ phase is not observed. This implies that 800 °C – calcined powders have no excess of titanium. For the presence of the CuO phase in both the samples of CCTO_EW700 and CCTO_EW800, it is possible that the Cu rich phase derives from the diffusion of Cu to the defects present, after which gross excess causes the crystallization of the separate CuO phase [42]. The CuO phase within the ceramics implies that excess copper is in the form of a copper rich phase at the grain boundaries [43]. The values of lattice parameter a calculated from the XRD spectra were 7.388 ± 0.001 and 7.393 ± 0.001 Å for the CCTO_EW700 and CCTO_EW800, respectively (see summary in Table 3).

Figure 7a and b show the real and imaginary parts of dielectric dispersion for the samples of CCTO_EW700 and CCTO_EW800 at various temperatures between −50 and −10 °C. It is clearly seen from Fig. 7a.1 and 7b.1 that both

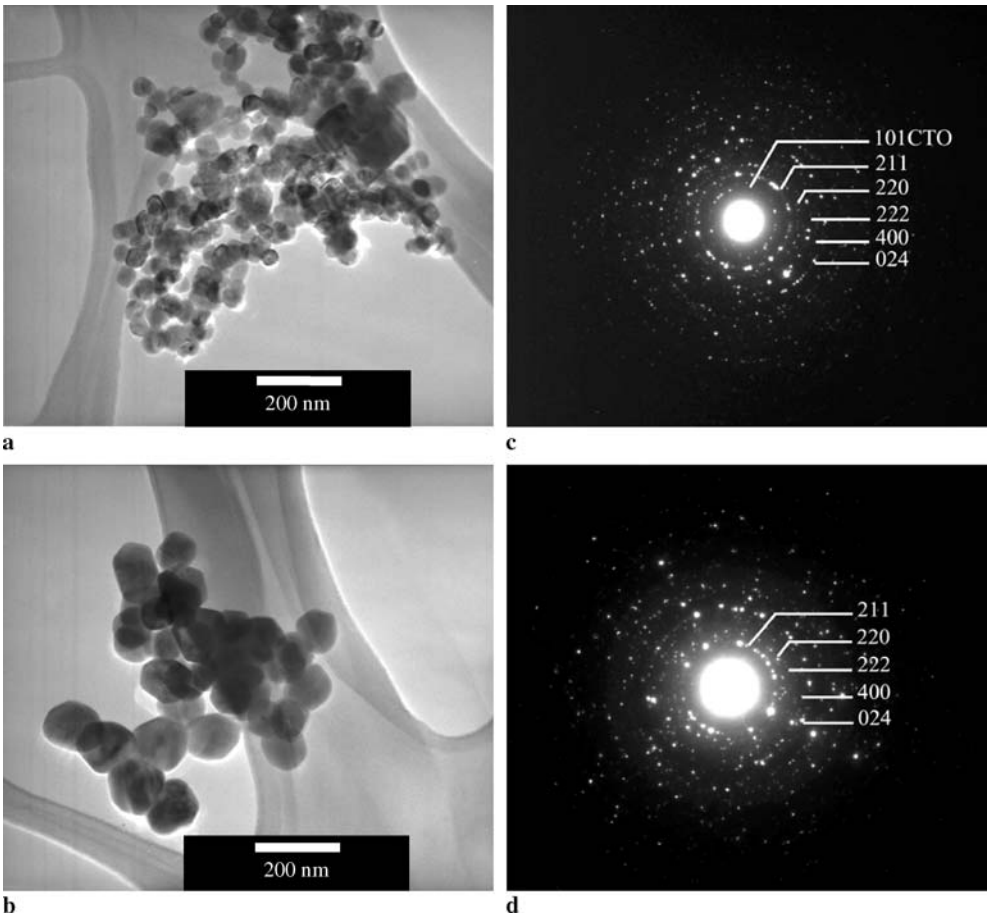

FIGURE 5 Bright field TEM images with corresponding selected-area electron diffraction (SAED) pattern of $CaCu_3Ti_4O_{12}$ powders calcined in air for 8 h at different temperatures: (**a**) 700 °C and (**b**) 800 °C (CTO-$CaTiO_3$)

samples have very high dielectric constant, ε', of $\sim 2.5 \times 10^4$ (at 1 kHz) for CCTO_EW700 and $\sim 1.5 \times 10^4$ (at 1 kHz) for CCTO_EW800. ε' has little frequency dependence at low frequency (below 100 kHz). Figure 8 compares the temperature dependence of the dielectric constant with the loss tangent at a frequency in the range of 100 Hz–1 MHz for the samples of CCTO_EW700 and CCTO_EW800. It is seen that the samples exhibits a giant dielectric constant, ε', $\sim 5 \times 10^4$ (at 1 kHz) for CCTO_EW700 (Fig. 7c.1) and $\sim 4 \times 10^4$ (at 1 kHz) for CCTO_EW800 (Fig. 7d.1) at 150–190 °C with weak frequency dependence above 1 kHz. The values of tan δ of both samples (Fig. 7c.2 for CCTO_EW700 and Fig. 7d.2 for CCTO_EW800) are high and are in the range of $\sim$ 0.2–30 at temperatures between −50 and 190 °C. These tan δ values increase with increasing temperature. The high ε' at low frequency may imply that there have grain boundary contributions in these sintered CCTO ceramics [44]. The values are similar to the those reported by Jin et al. [10] and Liu et al. [13] who reported values of $\varepsilon' \sim 10^4$ (at 1 kHz) for CCTO samples prepared from a solution route; and by Ramirez

Ring	Measured interplanar spacing of CCTO samples d_{hkl} (Å)		Standard data (JCPDS: 75-2188)	
	700 °C powder	800 °C powder	d_{hkl} (Å)	hkl
R_1	2.9719	2.9382	3.0173	211
R_2	2.5856	2.5456	2.6131	220
R_3	2.1021	2.1912	2.1336	222
R_4	1.8468	1.8469	1.8477	400
R_5	1.6789	1.6574	1.6526	024

TABLE 2 Measured interplanar spacings (d_{hkl}) obtained from selected-area electron diffraction patterns of CCTO samples calcined at 700, and 800 °C for 8 h shown in Fig. 5. Corresponding values from the standard data JCPDS: 75-2188 are also provided for a comparison

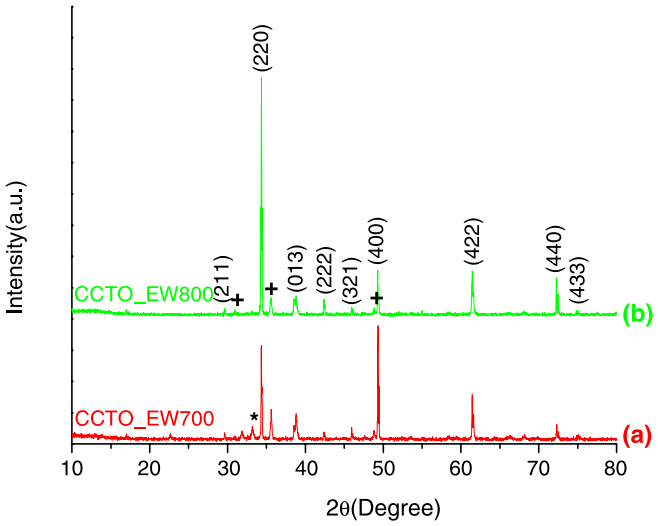

FIGURE 6 XRD patterns of (**a**) 700 °C; and (**b**) 800 °C, respectively. All sintering was done in air at 1100 °C for 16 h. The *indexed planes* indicated in all pattern are for CCTO main structure. (* – $CaTiO_3$ and + – CuO)

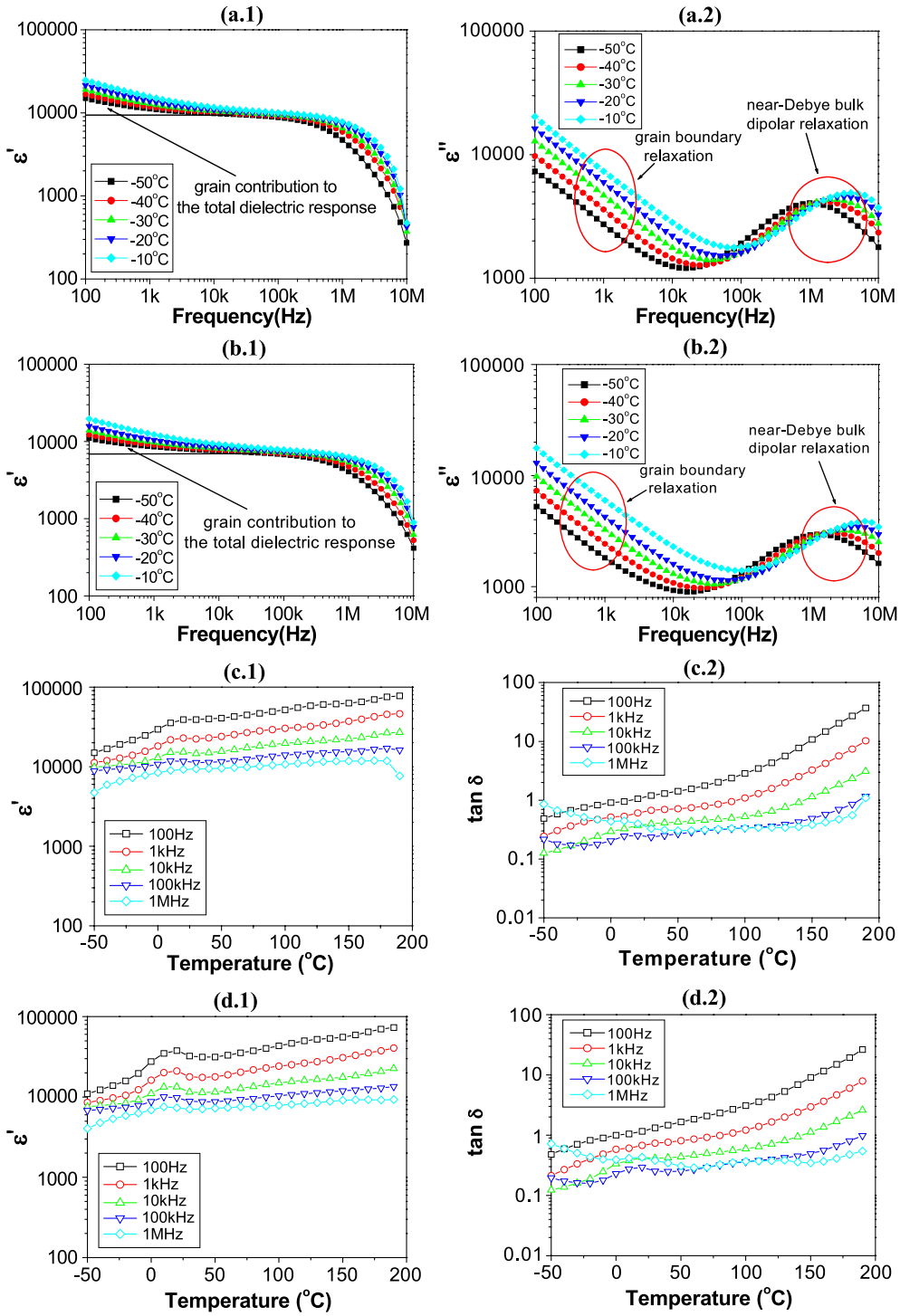

FIGURE 7 The frequency dependence of the complex permittivity, ε^*, at low temperature between $-50\,^{\circ}\mathrm{C}$ and $-10\,^{\circ}\mathrm{C}$ for CCTO_EW700 (**a.1** and **a.2**) and CCTO_EW800 (**b.1** and **b.2**), respectively. (**a.1**) and (**b.1**) display the real part ε'; (**a.2**) and (**b.2**) display the imaginary part ε''. The (**c.1**)-(**d.1**) and (**c.2**)-(**d.2**) show the temperature dependence of the dielectric constant, ε', and $\tan\delta$ at frequency between 100 Hz and 1 MHz for CCTO_EW700 (**c.1** and **c.2**) and CCTO_EW800 (**d.1**-**d.2**), respectively

Material	Grain size (μm)	Lattice parameter a (Å)	Activation energy of grains (eV)	Activation energy of grain boundaries (eV)
ASTM (75-2188)	–	7.391 ± 0.001	–	–
CCTO-EW700	12.0 ± 7.8	7.388 ± 0.001	0.175	0.680
CCTO-EW800	15.5 ± 8.9	7.393 ± 0.001	0.210	0.650

TABLE 3 Summary of grain size (from SEM), lattice parameter (from XRD), activation energy of grains (obtained from the curve fitting using (6)), and activation energy of grain boundaries (obtained from the curve fitting using (9)

et al. [1], and Bender and Pan [12], whose samples prepared from a solid state reaction method. These values, however, are much higher than $\sim 3 \times 10^3$ of the polymeric citrate precursor routed CCTO ceramics reported by Jha et al. [8].

The imaginary parts of dielectric dispersion, ε'' are shown in Fig. 7a.2 and b.2 for the samples of CCTO_EW700 and CCTO_EW800, respectively. By considering these results, we cannot apply the empirical Cole–Cole relation to fit these

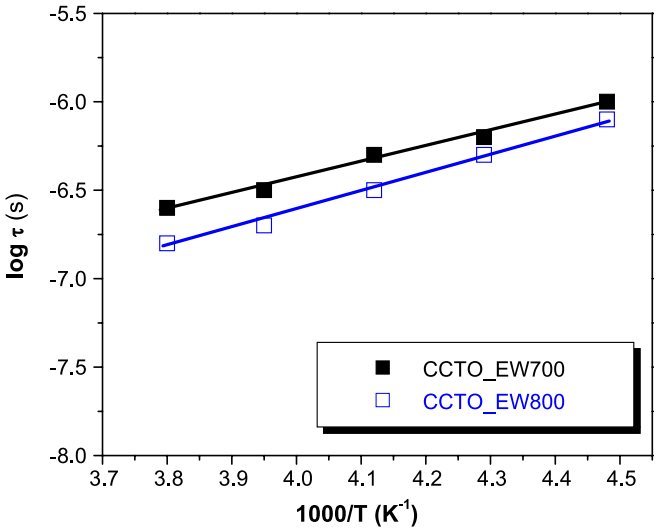

FIGURE 8 Arrhenius plot of the relaxation time for the sintered CCTO ceramics

data because the samples contain numerous grain boundaries or grain boundaries relaxation which was affected by low frequency [44]. However, we can apply the Debye-like relaxation model to these data since there are the relaxations contributed from the grains. The ε'' shows a clear Debye-like relaxation peak shifting from a constant value at low frequency to a small saturated value at higher frequency. The electrical response from the grains has a very high response frequency because of their small resistance and capacitance [13]. We can determine the dielectric relaxation time, τ, by following the Arrhenius law of

$$\tau = \tau_0 \exp\left(E_\tau / k_B T\right) , \tag{6}$$

where τ_0 is the pre-exponential factor, E_τ is the activation energy for the relaxation, k_B is the Boltzmann constant, and T is the absolute temperature. The activation energy of an electrical response, at different temperature can be derived from the response time ($\tau = 1/2\pi f$, where f is the response frequency at which the imaginary part of the complex impedance has a maximum). From the fitting shown in Fig. 8, we obtain the activation energy of the dielectric relaxation to be 0.175 eV for CCTO_EW700 and 0.210 eV for CCTO_EW800.

The ac conductivity, σ_{ac}, in most of the materials due to localized states may be described by [45]

$$\sigma_{ac} = \sigma_{dc} + A f^n , \tag{7}$$

where σ_{dc} is direct current conductivity. A, and n ($0 < n < 1$) are two temperature-dependent adjusting constants. From (7), the term of σ_{dc} presents the frequency independent part of the conductivity whereas the term of $A f^n$ is the frequency dependent part of the conductivity. However, our results did not fit well with (7) but the data can be fitted to equation

$$\sigma_{ac} = \sigma_{gb} + a f^t + \alpha f^2 , \tag{8}$$

where σ_{gb} is the dc gain boundary conductivity, a, t and α are three adjustable constants [45]. In (8), the $\sigma_{gb} + a f^t$ term describes the grain boundary conductivity relaxation [45]. The αf^2 term describes the transition between the two aforementioned relaxation behaviors [45, 46]. Figure 9 shows the log–log plot of ac conductivity versus frequency of the CCTO ceramics at five different temperatures. The solid lines in Fig. 9a and b are the fitted results of (8) with $t = 0.53$. For the CCTO_EW700, when the temperature increases from 150 °C to 190 °C, σ_{gb} and a increase from 3×10^{-6} to 1.5×10^{-5} S/cm and 9×10^{-8}–2.2×10^{-7} S/cm, respectively. For the CCTO_EW800, when the temperature increases from 150 °C to 190 °C, the values of σ_{gb} increases from 2×10^{-6}–9.5×10^{-6} S/cm, whereas the values of a rise from 7×10^{-8} to 2.2×10^{-7} S/cm. From the fitted results, we can obtain the dc gain boundary conductivity for the CCTO ceramics at different temperatures, and then we can fit σ_{gb} also by following the Arrhenius law of

$$\sigma_{gb} = \sigma_{gb}^0 \exp\left(-E_a / k_B T\right) , \tag{9}$$

where σ_{gb}^0 is the pre-exponential factor, E_a is the activation energy. From the fitting (Fig. 10), we obtain the activation energies of the dielectric relaxation for CCTO_EW700 and CCTO_EW800 to be 0.680 eV and 0.650 eV, respectively. These two values are comparable to the reported values of 0.60 eV [11] and 0.658–0.678 eV [18] for the grain bound-

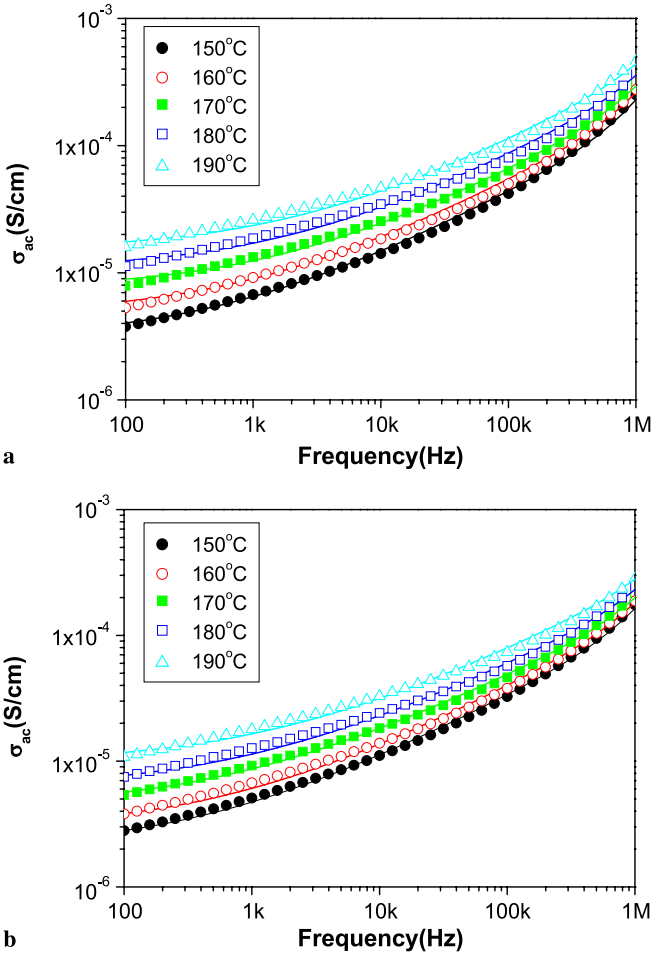

FIGURE 9 The frequency dependence of the ac conductivity, σ_{ac}, at high temperature ranging between 150 °C and 190 °C for (**a**) CCTO_EW700, and (**b**) CCTO_EW800, respectively. The *solid lines* are the fits according to (8)

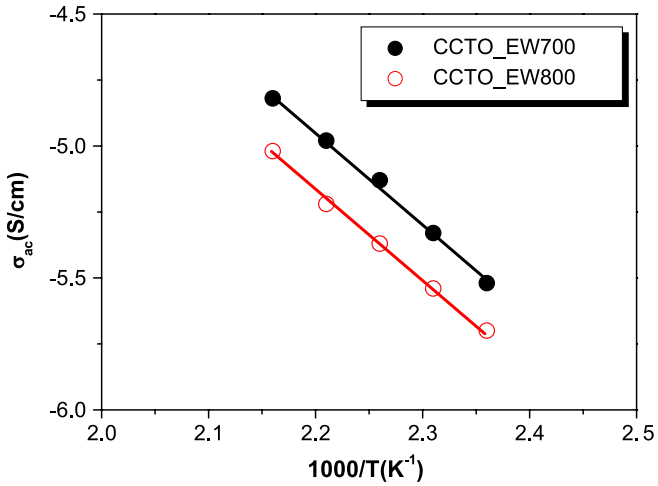

FIGURE 10 Arrhenius plot of ac conductivity, σ_{ac}, for the sintered CCTO ceramics

aries of CCTO ceramics. As mentioned previously, we have shown that the all CCTO ceramics are electrically inhomogeneous. It consists of semi-conducting grains and insulating grain boundaries, which can be described by the hypothesis of the existence of internal barrier layers between the grains.

Since the dielectric response in both CCTO_EW700 and CCTO_EW800 shows the Debye-like relaxation which is approximately equal to the pure Debye functional form of a Maxwell–Wagner relaxation, the giant dielectric behavior of both samples can be explained by using Maxwell–Wagner relaxation model. The Maxwell–Wagner relaxation can be described by an equivalent circuit consisting of a series array of two sub-circuits, one representing grain effects and one grain boundaries [11, 13]. In each sub-circuit, the resistor and capacitor are in parallel. From this equivalent circuit, the static permittivity (ε'_s) and dielectric relaxation time (τ) can be calculated as

$$\varepsilon'_s = \left(R_g^2 C_g + R_{gb}^2 C_{gb}\right) \Big/ \left[C_0 \left(R_g + R_{gb}\right)^2\right] \tag{10}$$

and

$$\tau = \left[R_g R_{gb} \left(C_g + C_{gb}\right)\right] / \left(R_g + R_{gb}\right), \tag{11}$$

where R_g, R_{gb} and C_g, C_{gb} are the resistance and capacitance of grains and grain boundaries, respectively [47]. Since $R_{gb} \gg R_g$, and C_{gb} is also much larger than C_g [11, 13], the effective dielectric permittivity (ε'_s) of the sample at frequencies much lower than the relaxation frequency $1/2\pi\tau$ can, therefore, be approximately from (10),

$$\varepsilon'_s = C_{gb}/C_0 . \tag{12}$$

Thus, ε'_s is determined by the ratio between grain boundary capacitance, C_{gb}, and empty cell capacitance, C_0. Hence ε'_s is constant when C_{gb} is temperature and frequency independent. The implication is in good agreement with our experimental results. We observed that dielectric constant is little dependent on the frequency and only weakly dependent on the temperature. And we can approximate τ from (11) using

$$\tau \approx R_g C_{gb} = \tau_g (C_{gb}/C_g) , \tag{13}$$

where $\tau_g = R_g C_g$ is the response time of the grains [13]. It has been reported that C_g and C_{gb} are independent of temperature [11, 13], thus, we can deduce τ_g that follows the Arrhenius law, (6). Let $\tau_g = \tau_g^0 \exp(E_g/k_B T)$ (τ_g^0 is pre-exponential factor and E_g is the activation energy of the grain conduction process), then we modify (13) to

$$\tau \approx \frac{C_{gb}}{C_g} \tau_g^0 \exp\left(E_g/k_B T\right) . \tag{14}$$

Equation (14) shows that the activation energy of the dielectric process approximately equals that of the grain conduction process. On the basis of this analysis, we can conclude that the activation energy for the response of the grains in CCTO_EW700, and CCTO_EW800 to be 0.175 eV and 0.210 eV, which are lager than the value (0.08 eV) reported by Sinclair et at. using solid-state reaction [11].

From all the activation energy values, we have that the grain boundaries of all CCTO ceramics have a much larger activation energy (0.680 eV for CCTO_EW700 and 0.650 eV for CCTO_EW800) than that of the grains (0.175 eV for CCTO_EW700 and 0.210 eV for CCTO_EW800). This indicates that the all CCTO ceramics have a high energy barrier for the charge carriers to overcome. Therefore, the grain boundaries exhibit insulating properties. In contrast, the smaller activation energy of grains displays semiconducting properties similar to occur in other titanate-based materials [48].

At this time, the origin of semi-conducting grains and insulating grain boundaries has not been clearly established. Liu et al. [13] have proposed that the grains made by different method could have very different electrical property. Therefore, the larger activation energy of grains in CCTO_EW700 and CCTO_EW800 compared to that of a sample made by solid-state reaction implies that there are fewer oxygen vacancies in the grains of CCTO_EW700 and CCTO_EW800. This is reasonable because CCTO_EW700 and CCTO_EW800 were sintered from powders, which were calcined at low temperature (700 and 800 °C) compared to the temperature needed for the solid-state processing. However, it is premature to associate the increase in grain activation energy of all CCTO ceramics with its large dielectric constant.

4 Conclusions

CCTO nano-powders have been synthesized by simple egg white solution route. The synthesized powders were characterized by TG-DTA, XRD, FTIR, SEM, and TEM. The powders calcined at 700 and 800 °C were used to prepared bulk CCTO ceramics, which were sinterred at 1100 °C for 16 h. The dielectric behaviour of CCTO ceramics were obtained to similar to that of CCTO made by solid state reaction, i.e., there are a Debye-like relaxation in the samples and their giant dielectric constant are little dependent of frequency and temperature below the relaxation frequency. The dielectric properties of these CCTO ceramics are attributed to the Maxwell–Wagner polarization mechanism. This work demonstrates that a simple solution route using water-soluble egg white proteins can be used for preparation of giant dielectric CCTO ceramics. We believe that

the current simple, cost effective and environmental friendly synthesis method using water-soluble egg white proteins can be extended to prepare fine particles of other interesting materials.

ACKNOWLEDGEMENTS The authors would like to thank the Department of Chemistry, Khon Kaen University for providing TG-DTA, the Faculty of Science Electron Microscopy Unit, Khon Kaen University for providing SEM facilities and the Department of Materials Science and Engineering, the University of Arizona for providing TEM. C. Masingboon would like to thank the University Staff Development Program, Kasetsart University Chalermphrakiat Sakon Nakhon Province Campus, Thailand for financial support of his PhD study. This work is financially supported by the Thailand Research Fund (TRF).

REFERENCES

1 A.P. Ramirez, M.A. Subramanian, M. Gardel, G. Blumberg, D. Li, T. Vogt, S.M. Shapiro, Solid State Commun. **115**, 217 (2000)
2 M.A. Subramanian, L. Dong, N. Duan, B.A. Reisner, A.W. Sleight, J. Solid State Chem. **151**, 323 (2000)
3 C.C. Homes, T. Vogt, S.M. Shapiro, S. Wakimoto, A.P. Ramirez, Science **293**, 73 (2001)
4 A.F.L. Almeida, R.S. de Oliveira, J.C. Góes, J.M. Sasaki, A.G. Souza Filho, J. Mendes Filho, A.S.B. Sombra, Mater. Sci. Eng. B **96**, 275 (2002)
5 M.A. Subramanian, A.W. Sleight, Solid State Sci. **4**, 347 (2002)
6 Z. Yu, C. Ang, J. Appl. Phys. **91**, 794 (2002)
7 L. Fang, M.R. Shen, Thin Solid Films **440**, 60 (2003)
8 P. Jha, A.K. Arora Pand Ganguli, Mater. Lett. **57**, 2443 (2003)
9 J. Li, A.W. Sleight, M.A. Subramanian, Solid State Commun. **135**, 260 (2005)
10 S. Jin, H. Xia, Y. Zhang, J. Guo, J. Xu, Mater. Lett. **61**, 1404 (2007)
11 D.C. Sinclair, T.B. Adams, F.D. Morrison, A.R. West, Appl. Phys. Lett. **80**, 2153 (2002)
12 B.A. Bender, M.J. Pan, Mater. Sci. Eng. B **117**, 339 (2005)
13 J. Liu, Y. Sui, C. Duan, W.N. Mei, R.W. Smith, J.R. Hardy, Chem. Mater. **18**, 3878 (2006)
14 P. Thongbai, C. Masingboon, S. Maensiri, T. Yamwong, S. Wongsaenmai, R. Yimnirun, J. Phys.: Condens. Matter **19**, 236208 (2007)
15 S. Maensiri, P. Thongbai, T. Yamwong, Appl. Phys. Lett. **90**, 202908 (2007)
16 S. Chung, I. Kim, S. Kang, Nat. Mater. **3**, 774 (2006)
17 T.T. Fang, H.K. Shiau, J. Am. Ceram. Soc. **87**, 2072 (2004)
18 S.F. Shao, J.L. Zhang, P. Zheng, W.L. Zhong, C.L. Wang, J. Appl. Phys. **99**, 084106 (2006)
19 P. Lunkenheimer, V. Bobnar, A.V. Pronin, A.I. Ritus, A.A. Volkov, A. Loidl, Phys. Rev. B **66**, 052105 (2002)
20 P. Lunkenheimer, R. Fichtl, S.G. Ebbinghaus, A. Loidl, Phys. Rev. B **70**, 172102 (2004)
21 M.H. Cohen, J.B. Neaton, L.X. He, D. Vanderbilt, J. Appl. Phys. **94**, 3299 (2003)
22 L. Zhang, Z.J. Tang, Phys. Rev. B **70**, 174306 (2004)
23 A.R. West, T.B. Adams, F.D. Morrison, D.C. Sinclair, J. Eur. Ceram. Soc. **24**, 1439 (2004)
24 G. Chiodeli, V. Massarotti, D. Capsoni, M. Bini, C.B. Azzoni, M.C. Mozzati, P. Lupotto, Solid State Commun. **132**, 241 (2004)
25 D. Capsoni, M. Bini, V. Massarotti, G. Chiodelli, M.C. Mozzatic, C.B. Azzoni, J. Solid State Chem. **177**, 4494 (2004)
26 S.V. Kalinin, J. Shin, G.M. Veith, A.P. Baddorf, M.V. Lobanov, H. Runge, M. Greenblatt, Appl. Phys. Lett. **86**, 102902 (2005)
27 T.T. Fang, L.T. Mei, H.F. Ho, Acta Mater. **54**, 2867 (2006)
28 B.L. Cushing, V.L. Kolesnichenko, C.J. O'Connor, Chem. Rev. **104**, 3893 (2004)
29 D.V. Vadehra, K.R. Nath, CRC Crit. Rev. Food. Technol. **4**, 193 (1973)
30 E. Li-Chen, S. Nakai, CRC Crit. Rev. Poultry Biol. 21 (1989)
31 Y. Mine, Trends Food Sci. Technol. **6**, 225 (1995)
32 O. Lyckfeldt, J. Brandt, S. Lesca, J. Eur. Ceram. Soc. **20**, 2551 (2000)
33 S. Dhara, P. Bhargava, J. Am. Ceram. Soc. **84**, 3045 (2001)
34 S. Dhara, P. Bhargava, J. Am. Ceram. Soc. **86**, 1645 (2003)
35 S. Dhara, J. Am. Ceram. Soc. **88**, 2003 (2005)
36 S. Maensiri, C. Masingboon, P. Laokul, W. Jareonboon, V. Promarak, P.L. Anderson, S. Seraphin, Cryst. Growth Design **7**, 950 (2007)
37 S. Maensiri, C. Masingboon, B. Boonchom, S. Seraphin, Scripta Mater. **56**, 797 (2006)
38 W. Li, R.W. Schwartz, Appl. Phys. Lett. **89**, 242906 (2006)
39 S. Guillemet-Fritsch, T. Lebey, M. Boulos, B. Durand, J. Eur. Ceram. Soc. **26**, 1245 (2006)
40 B.D. Cullity, S.R. Stock, *Elements of X-ray Diffraction* (Prentice Hall, Upper Saddle River, 2001)
41 C.L. Kretly, A.F.L. Almeida, P.B.A. Fechine, R.S. De Oliveira, A.S.B. Sombra, J. Mater. Sci. Mater. Electron. **15**, 657 (2004)
42 P. Leret, J.F. Fernandez, J. de Frutos, D. Fernández-Hevia, J. Eur. Ceram. Soc. **27**, 3901 (2007)
43 C.K. Yeoh, M.F. Ahmad, Z.A. Ahmad, J. Alloys Compd. **443**, 155 (2007)
44 M.A. Ramirez, P.R. Bueno, J.A. Varela, E. Longo, Appl. Phys. Lett. **89**, 212102 (2006)
45 L. Zhang, Appl. Phys. Lett. **87**, 022907 (2005)
46 S. Capaccioli, M. Lucchesi, P.A. Rolla, G. Ruggeri, J. Phys.: Condens. Matter **10**, 5595 (1998)
47 V. Hippel, *Dielectrics and Waves* (Wiley, New York, 1954)
48 F.D. Morrison, D.C. Sinclair, A.R. West, J. Am. Ceram. Soc. **84**, 474 (2001)